Supporting Information for

Atomically Layered and Ordered Rare-Earth *i*-MAX Phases: A New Class of Magnetic Quaternary Compounds

Quanzheng Tao[1*], Jun Lu[1], Martin Dahlqvist[1], Aurelija Mockute[1,2], Stuart Calder[2], Andrejs Petruhins[1], Rahele Meshkian[1], Oleg Rivin[3,4], Daniel Potashnikov[5,6], El'ad Caspi[3], Hagai Shaked[7], Andreas Hoser[4], Christine Opagiste[8], Rose-Marie Galera[8], Ruslan Salikhov[9], Ulf Wiedwald[9], Clemens Ritter[10], Andrew R. Wildes[10], Börje Johansson[11,12], Lars Hultman[1], Michael Farle[9], Michel W. Barsoum[1,13], Johanna Rosen[1*]

[1]Thin Film Physics Division, Department of Physics, Chemistry, and Biology (IFM), Linköping University, SE-581 83 Linköping, Sweden

[2]Neutron Scattering Division, Oak Ridge National Laboratory, Oak Ridge, Tennessee 37831, USA

[3]Physics Department, Nuclear Research Centre - Negev, P. O. Box 9001 Beer-Sheva 84190, Israel

[4]Helmholtz-Zentrum Berlin fur Materialen und Energie, Berlin 14109, Germany

[5]Faculty of Physics, Technion-Israeli Institute of Technology, Haifa 32000, Israel

[6]Israel Atomic Energy Commission, P. O. Box 7061, Tel-Aviv 61070, Israel

[7]Physics Department, Ben-Gurion University of the Negev, P. O. Box 653 Beer-Sheva 84105, Israel

[8]Institut Neel, CNRS, Univ. Grenoble Alpes, Grenoble INP, FR-38000 Grenoble, France

[9]Faculty of Physics and Center for Nanointegration (CENIDE), University of Duisburg-Essen, 47057 Duisburg, Germany

[10]Institut Laue-Langevin, B P 156, 38042 Grenoble Cedex 9, France

[11]Department of Physics and Astronomy, Uppsala University, Box 516, SE-751 20 Uppsala, Sweden

[12]Humboldt University, Physics Department, Zum Grossen Windkanal 6, D-12489 Berlin, Germany

[13]Department of Materials Science and Engineering, Drexel University, Philadelphia, Pennsylvania 19104, USA.

Section S1. Structure analysis by STEM and XRD

a $(Mo_{2/3}Pr_{1/3})_2AlC$ *C*2/*m*

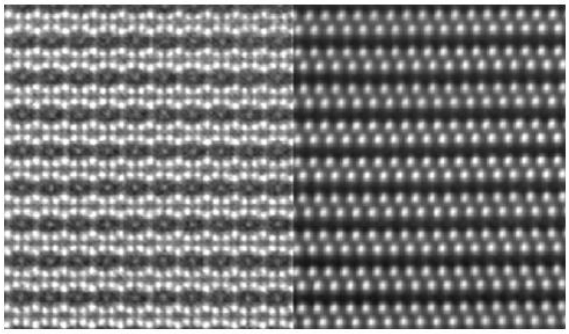

b $(Mo_{2/3}Nd_{1/3})_2AlC$ *C*2/*c*

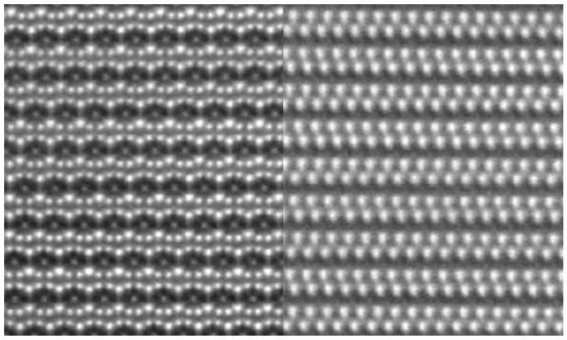

c $(Mo_{2/3}Sm_{1/3})_2AlC$ *C*2/*c*

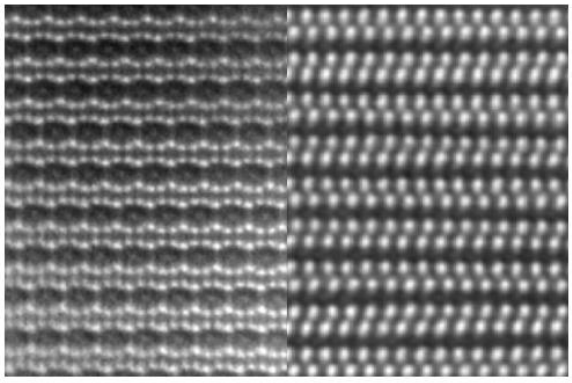

d $(Mo_{2/3}Sm_{1/3})_2AlC$ *C*2/*m*

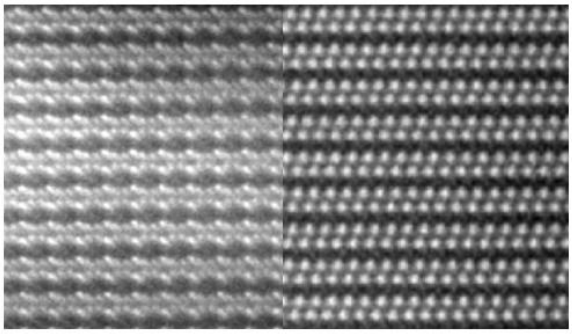

e $(Mo_{2/3}Gd_{1/3})_2AlC$ *C*2/*c*

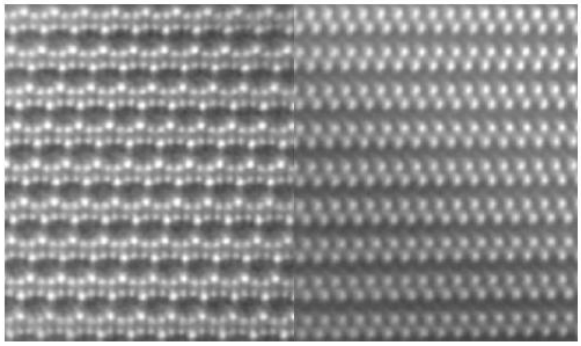

f $(Mo_{2/3}Dy_{1/3})_2AlC$ *C*2/*c*

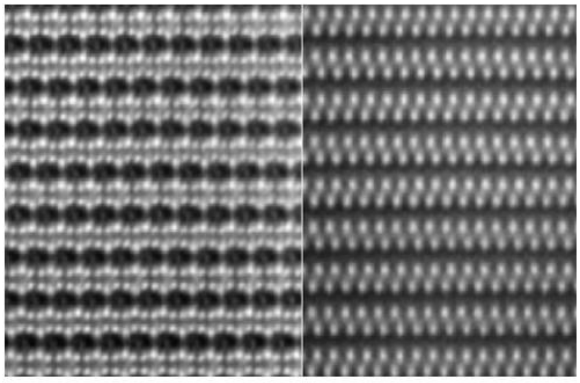

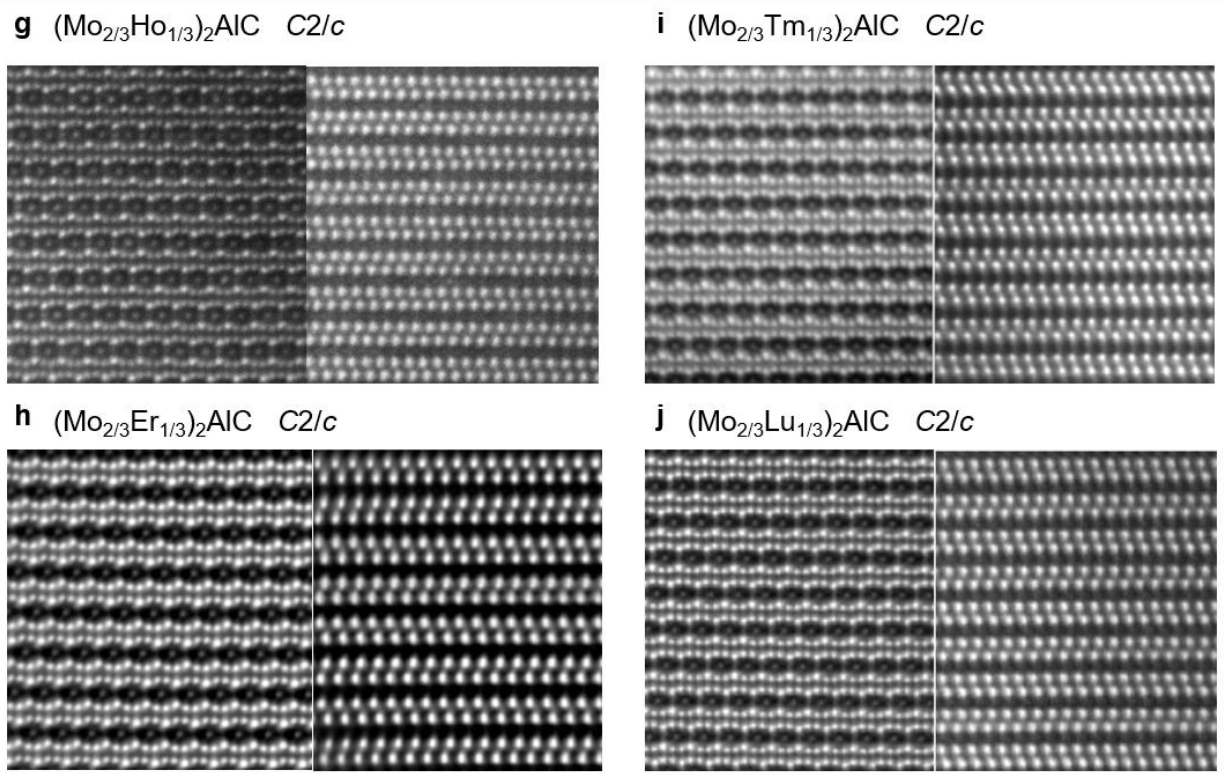

Fig. S1. **Crystal structure of RE *i*-MAX.** STEM images of RE=Ce, Pr, Nd, Sm, Gd, Dy, Ho, Er, Tm, Lu.

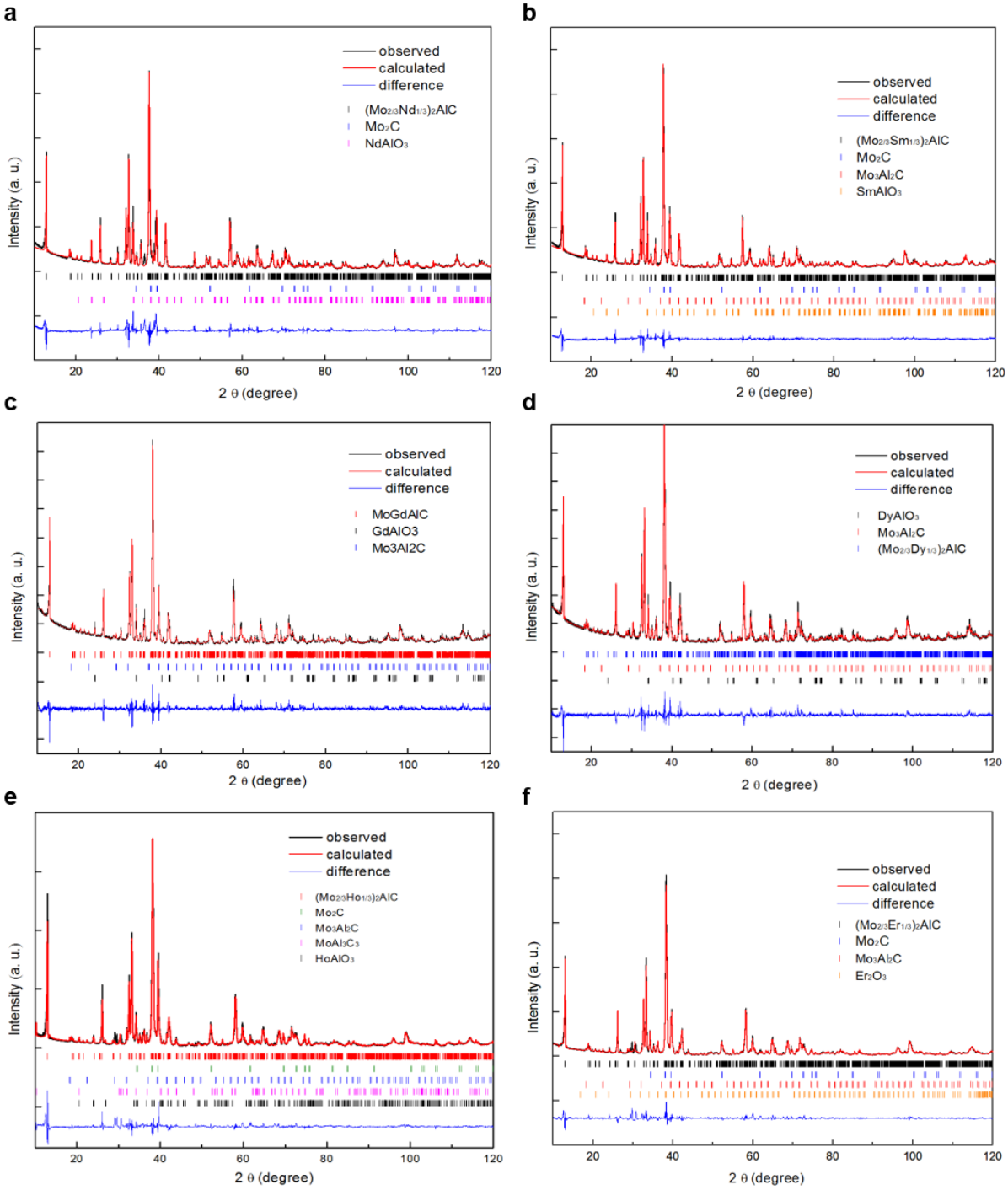
a
observed
calculated
difference
(Mo2/3Nd1/3)2AlC
Mo2C
NdAlO3
Intensity (a. u.)
2 θ (degree)
b
observed
calculated
difference
(Mo2/3Sm1/3)2AlC
Mo2C
Mo3Al2C
SmAlO3
Intensity (a. u.)
2 θ (degree)
c
observed
calculated
difference
MoGdAlC
GdAlO3
Mo3Al2C
Intensity (a. u.)
2 θ (degree)
d
observed
calculated
difference
DyAlO3
Mo3Al2C
(Mo2/3Dy1/3)2AlC
Intensity (a. u.)
2 θ (degree)
e
observed
calculated
difference
(Mo2/3Ho1/3)2AlC
Mo2C
Mo3Al2C
MoAl3C3
HoAlO3
Intensity (a. u.)
2 θ (degree)
f
observed
calculated
difference
(Mo2/3Er1/3)2AlC
Mo2C
Mo3Al2C
Er2O3
Intensity (a. u.)
2 θ (degree)

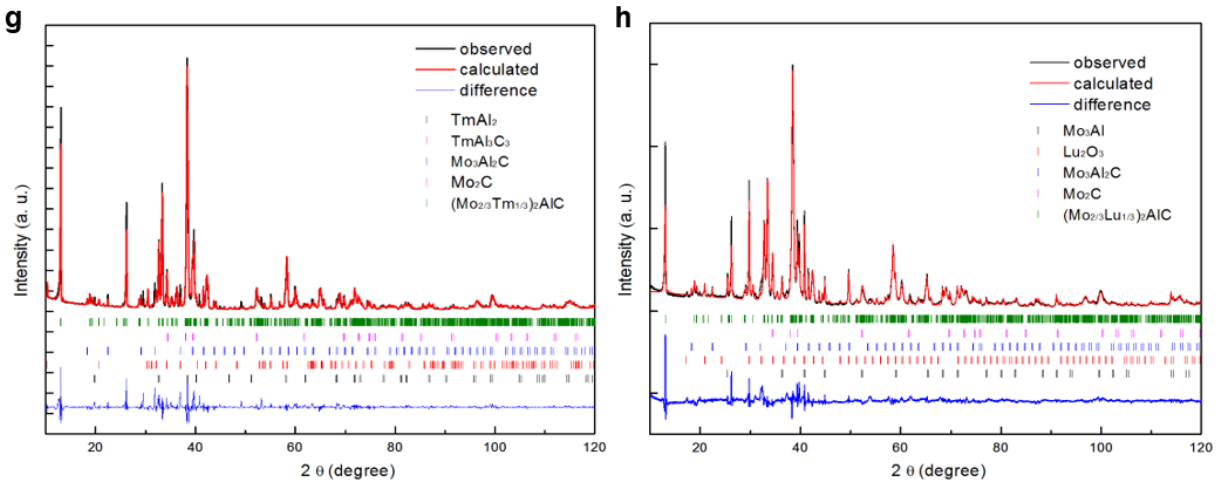

Fig. S2. **a-f** Rietveld refinement of XRD for RE= Nd, Sm, Gd, Dy, Ho, Er, Tm, Lu.

The XRD patterns from the samples containing Ce and Pr showed them to be of too low phase purity to motivate a detailed refinement. Furthermore, these *i*-MAX phases were accompanied with the ferromagnetic $RE_4Mo_4Al_7C_3$ and the nonmagnetic Mo_2C and $REAlO_3$ phases, hindering detailed magnetization analysis.

Table S1. Cell parameters and atom coordinates obtained from XRD Rietveld refinement at RT.

Space group	*C2/c (#15)*	*C2/c (#15)*	*C2/c (#15)*	*C2/c (#15)*	*C2/c (#15)*
RE	Nd	Sm	Gd	Tb	Dy
χ^2	29.2	12.4	6.6	7.7	6.4
a (Å)	*a* 9.66570 (10)	*a* 9.61514 (8)	*a* 9.57673 (12)	*a* 9.54627 (8)	*a* 9.52628 (10)
b (Å)	*b* 5.59353 (6)	*b* 5.56482 (5)	*b* 5.54259 (6)	*b* 5.52473(5)	*b* 5.51408 (5)
c (Å)	*c* 14.17243 (13)	*c* 14.12072 (11)	*C 14.09418* (16)	*c* 14.06829 (12)	*c* 14.04969 (14)
α	90	90	90	90	90
β	103.48465(69)	103.52045(53)	103.53428(82)	103.53555(62)	103.53767(69)
γ	90	90	90	90	90
RE	8f (0.95833(29) 0.41825(63) 0.12101(14))	8f (0.96127(15) 0.42102(34) 0.12001(7))	8f (0.96189(28) 0.41552(67) 0.12100(13),	8f (0.95948(21), 0.41824(53), 0.11744(11))	8f (0.96183(23) 0.42445(58) 0.11833(12))
Mo	8f (0.26981(45) 0.43116(83) 0.07611(19)) 8f (0.60799(39) 0.41324(94) 0.07398(18))	8f (0.60793(21) 0.40602(49) 0.07686(9)) 8f (0.27080(25) 0.42406(52) 0.07669(9))	8f (0.27093(43) 0.42028(92) 0.07794(17)) 8f (0.60976(39) 0.41053(88) 0.07992(15))	8f (0.27021(32), 0.41601(74), 0.07950(15)) 8f (0.60740(28), 0.40992(67), 0.07954(14))	8f (0.27173(37) 0.42346(82) 0.07922(17)) 8f (0.60919(33) 0.41425(75) 0.07949(16))
Al	8f (0.74535(136) 0.14219(264) 0.25375(90)) 4e (0.00000(0) 0.89498(350) 0.25000(0)	8f (0.75084(77) 0.15562(145) 0.25598(48)) 4e (0.00000(0) 0.91541(204) 0.25000(0))	8f (0.73895(135) 0.15809(272) 0.25744(81)) 4e (0.00000(0) 0.92446(355) 0.25000(0))	8f (0.74760(116), 0.16653(224), 0.25031(66)) 4e (0.00000, 0.91889(293), 0.25000)	8f (0.75544(110) 0.14299(200) 0.24995(71)) 4e (0.00000(0) 0.92469(309) 0.25000(0))
C	8f (0.40600 0.26952 0.00000) 4d (0.25, 0.25, 0.50)	8f (0.40600 0.26952 0.00000) 4d (0.25, 0.25, 0.50)	8f (0.41481, 0.23022, 0.0000) 4d (0.25, 0.25, 0.50)	8f (0.41481, 0.23022, 0.0000) 4d (0.25, 0.25, 0.50)	8f (0.41481, 0.23022, 0.0000) 4d (0.25, 0.25, 0.50)

C2/c (#15)	*C2/c (#15)*	*C2/c (#15)*	*C2/c (#15)*
Ho	Er	Tm	Lu
23.1	19.0	85.3	23.5
a 9.51198 (9)	*a* 9.49271 (11)	*a* 9.47697 (12)	*a* 9.44912 (23)
b 5.50274 (5)	*b* 5.49282 (6)	*b* 5.48572 (7)	*b* 5.47033 (13)
c 14.03831 (13)	*c* 14.01770 (15)	*c* 14.00152 (17)	*C 13.97305* (28)
90	90	90	90
103.54111(69)	103.53001(66)	103.51039(92)	103.48195(166)
90	90	90	90
8f (0.95804(22) 0.41472(54) 0.11384(11))	8f (0.95802(20) 0.42234(47) 0.11485(9))	8f (0.95779(27) 0.42251(62) 0.11326(14))	8f (0.95760(33) 0.42200(75) 0.111609(14))
8f (0.27422(32) 0.42187(72) 0.07969(15))	8f (0.27571(29) 0.41851(73) 0.08114(14))	8f (0.27500(45) 0.42032(97) 0.07995(21))	8f (0.27592(59) 0.41943(125) 0.08670(106))
8f (0.60923(30) 0.40790(71) 0.07878(14))	8f (0.60960(27) 0.41194(65) 0.08095(13))	8f (0.61040(41) 0.40852(88) 0.08070(20))	8f (0.60313(175) 0.39619(346) 0.08390(94))
8f (0.73641(105) 0.19293(178) 0.24889(64))	8f (0.73793(106) 0.15368(224) 0.25207(59))	8f (0.75967(129) 0.13616(247) 0.25761(83))	8f (0.75230(482) 0.11147(1074) 0.25366(350))
4e (0.00000(0) 0.91073(297) 0.25000(0))	4e (0.00000(0) 0.91088(258) 0.25000(0))	4e (0.00000(0) 0.92483(381) 0.25000(0))	4e (0.00000(0) 0.96327(1570) 0.25000(0))
8f (0.41481, 0.23022, 0.0000)	8f (0.41481, 0.23022, 0.0000)	8f (0.41481, 0.23022, 0.0000)	8f (0.41481, 0.23022, 0.0000)
4d (0.25, 0.25, 0.50)	4d (0.25, 0.25, 0.50)	4d (0.25, 0.25, 0.50)	4d (0.25, 0.25, 0.50)

Table S2. Phase purity from Rietveld refinement in weight %.

RE	i-MAX	Mo_2C	Mo_3Al_2C	$REAlO_3$	$REAl_3C_3$	Others
Nd	88.5	6.8	N/A	4.7	N/A	N/A
Sm	94.5	4.5	1.0	N/A	N/A	N/A
Gd	94.4	N/A	4.4	1.2	N/A	N/A
Tb	98.1	1.9	N/A	N/A	N/A	N/A
Dy	95.1	N/A	4.0	0.9	N/A	N/A
Ho	83.0	6.8	2.4	3.8	4.04	N/A
Er	91.7	2.0	4.5	1.8	N/A	1.79 Er_2O_3
Tm	88.5	1.3	6.0	N/A	2.6	1.55 $TmAl_2$
Lu	70.9	2.6	7.9	N/A	N/A	8.3 Mo_3Al 10.3 Lu_2O_3

The Mo containing impurities observed in most samples, Mo_2C and Mo_3Al_2C, are paramagnetic. $NdAlO_3$ is antiferromagnetic below 0.93 K[1], and the magnetic transition observed at 7.6 K is therefore attributed to $(Mo_{2/3}Nd_{1/3})_2AlC$.

For the $(Mo_{2/3}Sm_{1/3})_2AlC$ sample, the magnetization is very weak and no magnetic transition can be observed down to 2 K. For the $(Mo_{2/3}Gd_{1/3})_2AlC$ sample, $GdAlO_3$ orders below 3.69 K[2], and the magnetic transition observed at 26 K is therefore attributed to the *i*-MAX phase.

For $(Mo_{2/3}Tb_{1/3})_2AlC$, only ~2% of Mo_2C can be found, and the two magnetic transitions can therefore be attributed to the *i*-MAX phase. We also clarified the mechanism of the two magnetic transitions by NPD.

$DyAlO_3$ orders at 3.52 K[3], and can therefore be excluded as origin to the observed magnetic characteristics. The behavior of $(Mo_{2/3}Dy_{1/3})_2AlC$ is also very similar to that of $(Mo_{2/3}Tb_{1/3})_2AlC$.

$HoAlO_3$ is antiferromagnetic below 0.16 K[4]. The magnetism of $HoAl_3C_3$ is unknown. Er_2O_3 orders at 3.36 K [5]. The magnetic contribution of Er_2O_3 to the NPD was considered following ref. 5.

No magnetic transition can be observed down to 2 K in the $(Mo_{2/3}Tm_{1/3})_2AlC$ sample. The $(Mo_{2/3}Lu_{1/3})_2AlC$ Lu sample is not analyzed with respect to magnetism.

Section S2. Relationship between three polymorphs

The three polymorphs identified possess the same $(Mo_{2/3}RE_{1/3})_2C$ layers as building blocks (**Fig. 1b**), with the difference between them being the layer stacking along the *c* axis. In the *C*2/*c* structure the layers are stacked in an ABAB sequence, and are rotated 60° with respect to each other, see **Fig. S3** for a schematic. In the *Cmcm* structure, on the other hand, the layers are stacked in an ACAC sequence, and are rotated 180° with respect to each other. In the *C*2/*m* structure, the layers are stacked exactly on top of each other, viz. the stacking is AAAA.

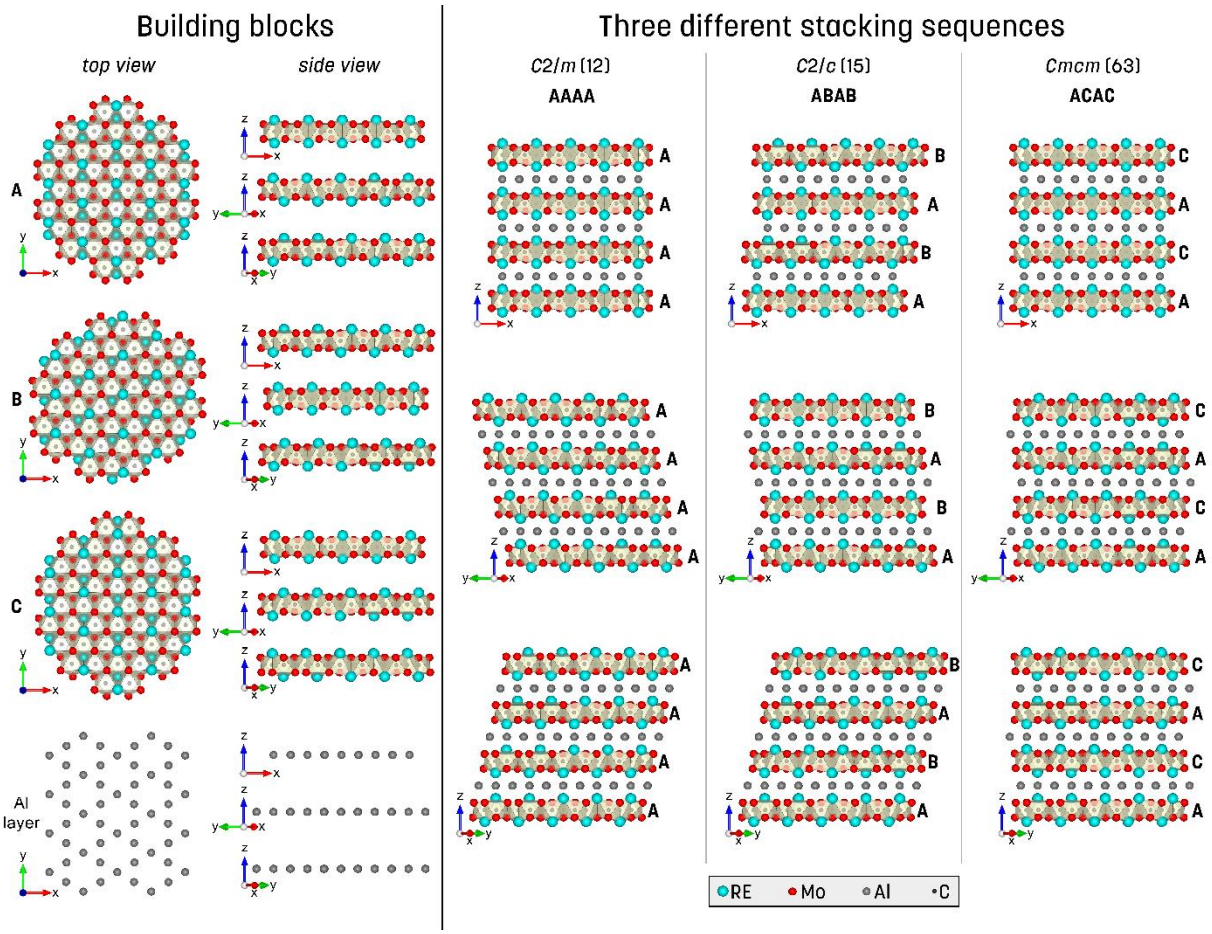

Fig. S3. Schematic illustration of different stacking sequences for REMAX in space group *C*2/*m* (12), *C*2/*c* (15), and *Cmcm* (63). The structure consists of alternating layers of $(Mo_{2/3}RE_{1/3})_2C$ and Al building blocks where $(Mo_{2/3}RE_{1/3})_2C$ can have three different orientations; **A**, **B** (rotated +60° relative **A**), and **C** (rotated +180° relative **A**). Different stacking sequences of $(Mo_{2/3}RE_{1/3})_2C$ results in *C*2/*c* structure with **AAAA** stacking, *C*2/*m* structure with **ABAB** stacking, and *Cmcm* structure with **ACAC** stacking.

Section S3. Theoretical modeling

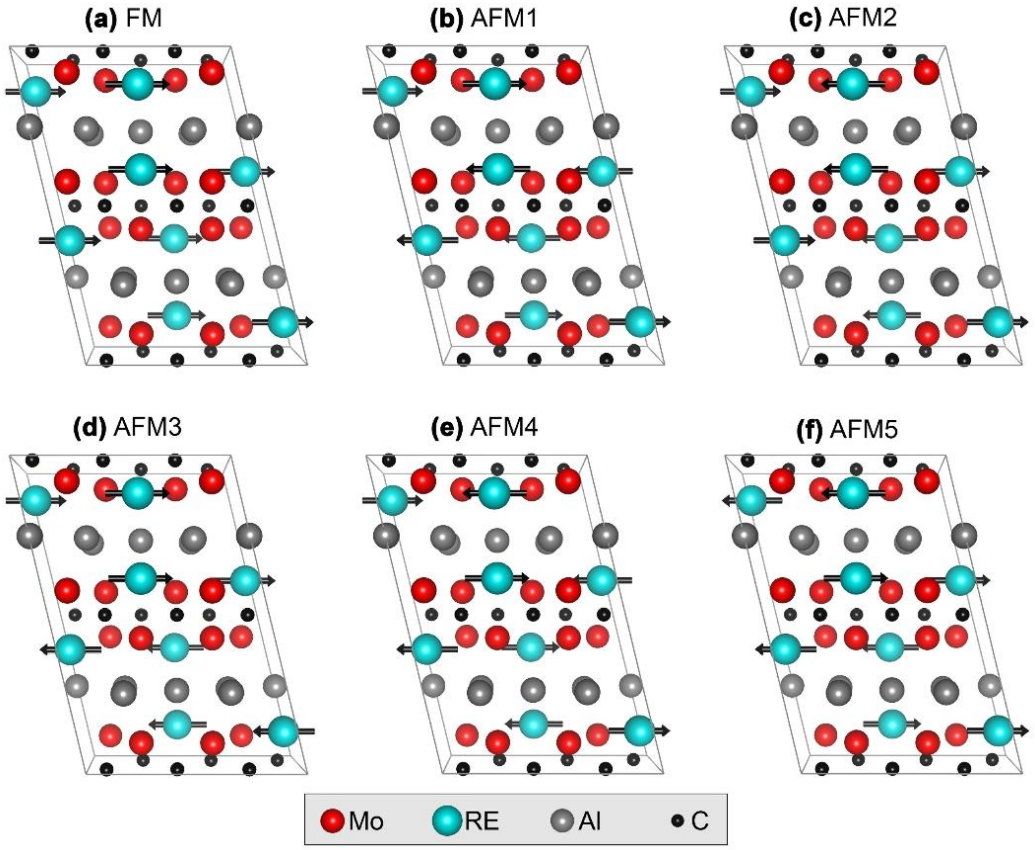

Fig. S4. Schematic representation of six collinear spin configurations considered for $(Mo_{2/3}RE_{1/3})_2AlC$ where the spin direction at each RE site is represented by a black arrow.

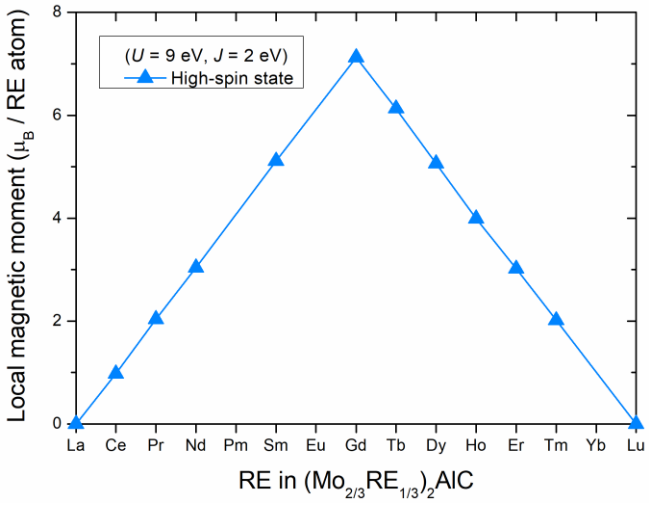

Fig. S5. Local magnetic moment of RE for $(Mo_{2/3}RE_{1/3})_2AlC$ with U= 9 eV and J= 2 eV.

Section S4. Curie-Weiss fitting in the paramagnetic state

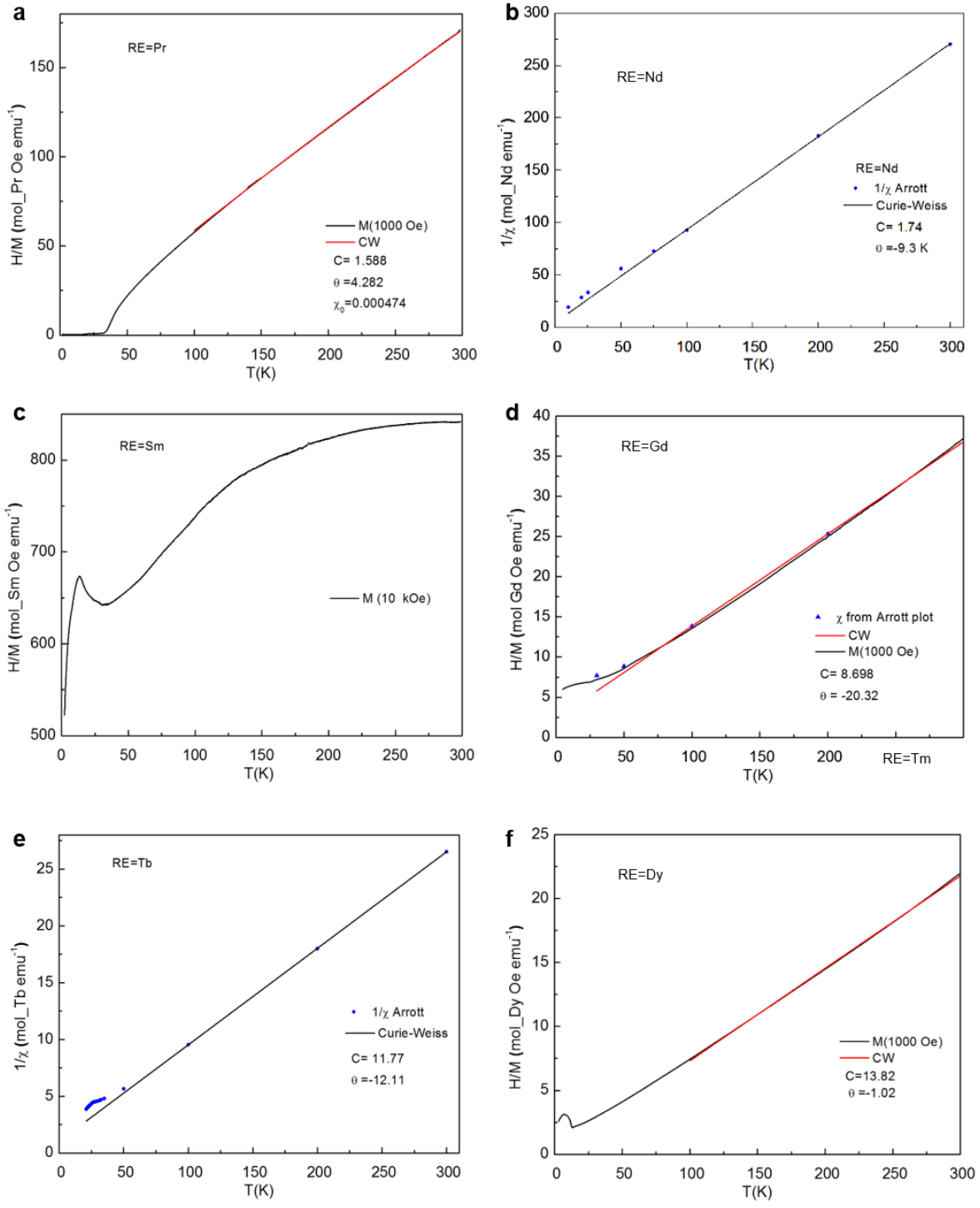

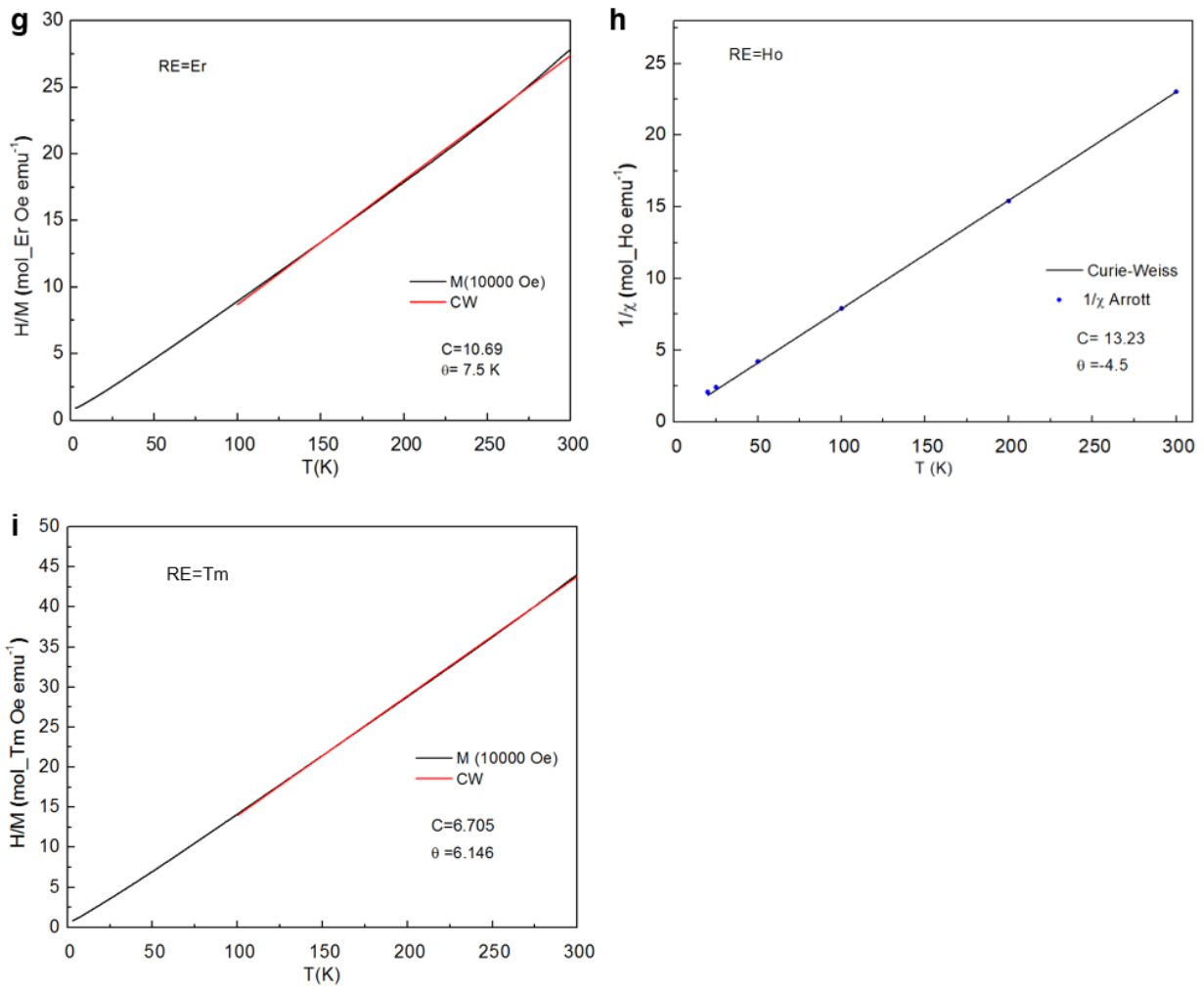

Fig S6. a-i H/M vs. T for RE = Pr, Nd, Sm, Gd, Tb, Dy, Er, Ho, and Tm, and their fitting to the Curie-Weiss law.

Supplementary Fig. 6 plots the inverse susceptibility 1/χ (deduced from Arrott plots) or H/M vs. T plots for 9 RE phases. In all cases, but Sm, a Curie-Weiss, C-W, law of the form

$$\chi = C/(T-\theta), \qquad (1)$$

where C is the Curie constant and T and θ are the temperature in K and the Curie-Weiss temperature, respectively. The resulting parameters are listed in **Fig. 4e**. The effective moment μ_{eff} per RE element is estimated from

$$C = N\mu_B^2\mu_{eff}^2/3k_B, \qquad (2)$$

where N is the number of magnetic atoms per unit volume, μ_B the Bohr magneton and k_B, Boltzmann's constant. All phases, except RE = Sm, fit well to **Eq. 1** in the 100 K~300 K temperature interval.

Section S5. Properties of $(Mo_{2/3}Gd_{1/3})_2AlC$ and $(Mo_{2/3}Tb_{1/3})_2AlC$

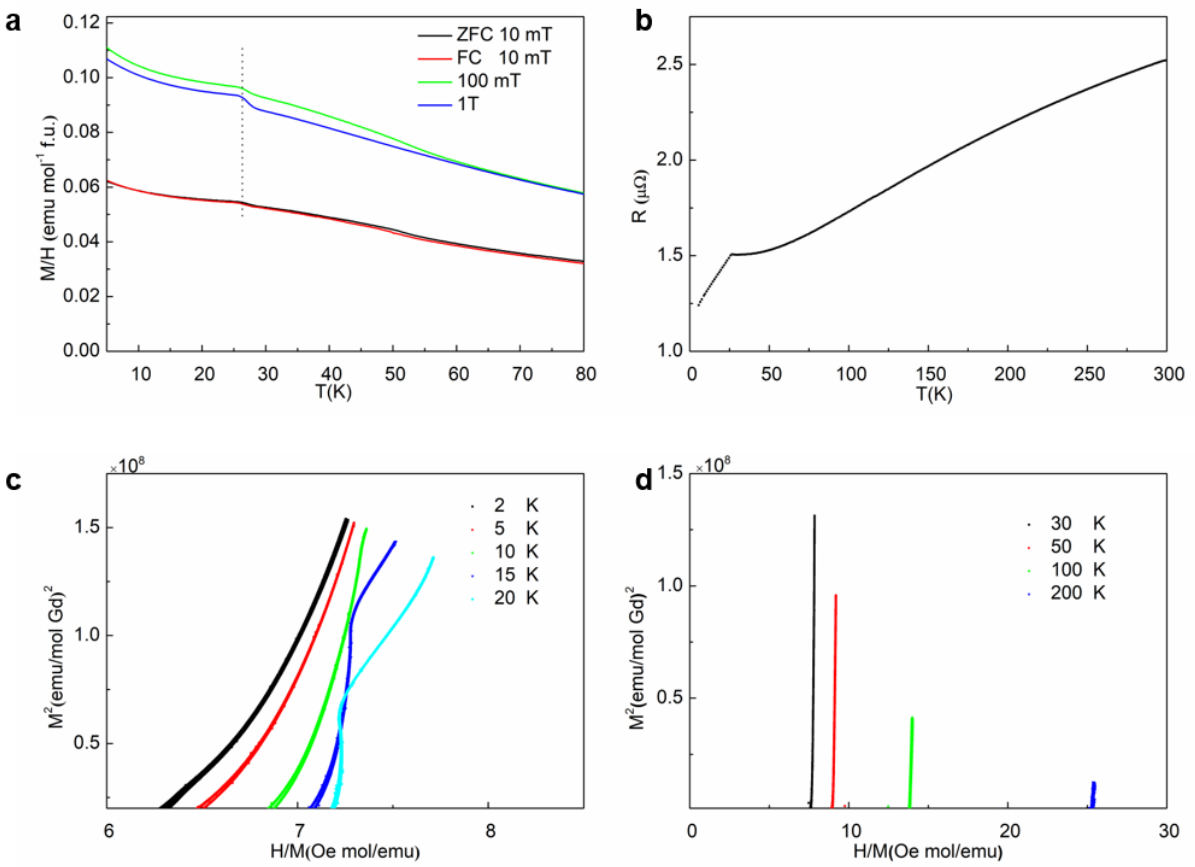

Fig. S7. **a**. M/H of $(Mo_{2/3}Gd_{1/3})_2AlC$. A weak bump is observed at T_N=26 K. **b**. Resistance vs. Temperature. **c**. Arrott plots above the transition temperature. **d**. Arrott plots below transition temperature.

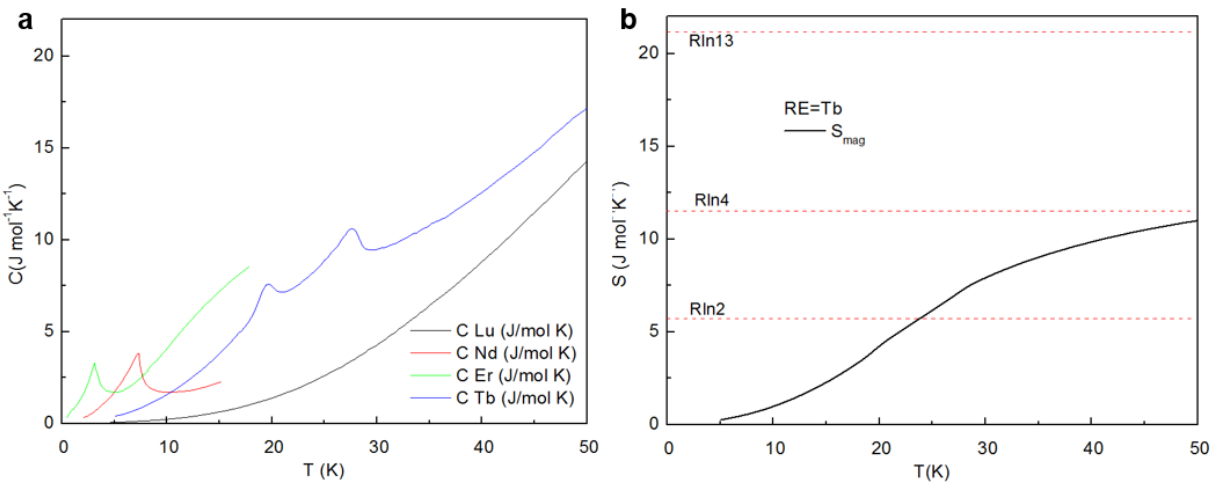

Fig S8. **a**. Heat capacity of RE=Lu, Tb, Nd, and Er. **b**. Thermal variation of magnetic entropy. The phonon contribution is subtracted by the non-magnetic analog RE=Lu. R ln2 is indicated by dashed line.

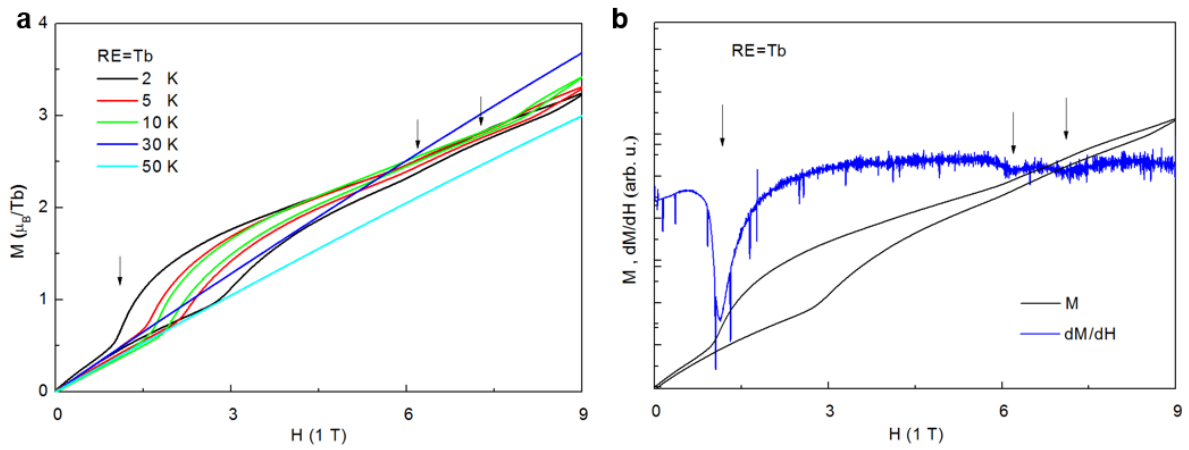

Fig S9. a. M-H at different temperatures for $(Mo_{2/3}Tb_{1/3})_2AlC$. **b**. dM/dH plot for $(Mo_{2/3}Tb_{1/3})_2AlC$ at 2 K. Arrows indicate field induced transitions.

Section S6. Detailed magnetic structure analysis of the NPD data

$(Mo_{2/3}Tb_{1/3})_2AlC$

Using the k-search program, the propagation vector for the structure below 20 K is indexed to be **k**=(0, 1/2, 0). The magnetic unit cell is twice the size of the nuclear cell. The symmetry analysis is performed by using the program BasIreps. The list of the irreducible representations is given in the table below. Note that the tables are only referred in this section, so they are numbered in Roman numbers. The magnetic representation can be decomposed:

$$\Gamma = 6\,\Gamma_1 \oplus 6\,\Gamma_2$$

Table Ⅰ. Irreducible representations. p=1/2.

Irreps	{1}	$\{2_y\|00p\}$	{-1}	$\{m_y\|00p\}$
Γ_1	$\begin{matrix}1 & 0\\ 0 & 1\end{matrix}$	$\begin{matrix}1 & 0\\ 0 & 1\end{matrix}$	$\begin{matrix}1 & 0\\ 0 & -1\end{matrix}$	$\begin{matrix}1 & 0\\ 0 & -1\end{matrix}$
Γ_2	$\begin{matrix}1 & 0\\ 0 & 1\end{matrix}$	$\begin{matrix}-1 & 0\\ 0 & -1\end{matrix}$	$\begin{matrix}1 & 0\\ 0 & -1\end{matrix}$	$\begin{matrix}-1 & 0\\ 0 & 1\end{matrix}$

Table Ⅱ. Basis vectors of Tb atoms

Irrep.	Basis vector	Tb1 (x,y,z)	Tb2 (-x,y,-z+1/2)	Tb3 (-x,-y,-z)	Tb4 (x,-y,z+1/2)
Γ_1	V_1	[100]	[-100]	[100]	[-100]
	V_2	[010]	[010]	[010]	[010]
	V_3	[001]	[00-1]	[001]	[00-1]
	V_4	[100]	[-100]	[-100]	[100]
	V_5	[010]	[010]	[0-10]	[0-10]
	V_6	[001]	[00-1]	[00-1]	[001]
Γ_2	V_1	[100]	[100]	[100]	[100]
	V_2	[010]	[0-10]	[010]	[0-10]
	V_3	[001]	[001]	[001]	[001]
	V_4	[100]	[100]	[-100]	[-100]
	V_5	[010]	[0-10]	[0-10]	[010]
	V_6	[001]	[001]	[00-1]	[00-1]

A trial and error method is used to determine the correct magnetic model. The *irreps* Γ_2 appears to be the correct solution. We have tried all possible magnetic models. The V_1 and V_3 appears to be the dominant vectors. In Table III, we summarized parameters obtained from refinement for the 8 K data by considering different magnetic models. As can be seen, the best agreement is achieved by considering V_1, V_2, and V_3. The R_{mag} =6.23 % is slightly better than R_{mag} =7.18 % considering V_1 and V_3. The refined magnetic moment is close to 5.0 (2) μ_B.

Table III. Parameters from refinement of 8 K data by considering different models of Γ_2.

V1	V2	V3	V4	V5	V6	R-mag (%)	M (μB)	M(μB)
-3.448	**0.551**	**2.839**	**0**	**0**	**0**	**6.23**	**4.9**	
-3.438	0	2.875	0.407	0	0	6.99	4.641	5.313
-3.432	0	2.885	0	0.379	0	6.92	4.988	
-3.443	0	2.867	0	0	0.417	7.01	4.67	5.285
-3.44	0	2.884	0	0	0	7.18	4.98	
-3.442	0.529	2.83	0.279	0.363	0.334	6.26	5.049	4.945

Similarly, we indexed the propagation vector for the structure at 22 K by k-search. No commensurate solution was found. The best solution is **k**=(0, ~0.6, 0). The symmetry for **k**=(0, ~0.6, 0) is the same as **k**=(0, 0.5, 0). Similarly, a trial and error is used to determine the correct solution. *Irreps* Γ_2 is the correct solution.

Table IV. Parameters from refinement of 22 K data by considering different models of Γ_2. M corresponds to the peak moment of the modulated structure.

V1	V2	V3	V4	V5	V6	R-mag %	M (μB)	$\boldsymbol{k}$=(0,δ,0)
2.807	-0.462	-2.599	0	0	0	12.37	4.27	0.6053
2.741	0	-2.669	0.877	0	0	12.16	4.973	0.6054
2.737	0	-2.646	0	-0.979	0	12.17	4.341	0.6053
2.787	0	-2.614	0	0	0.705	12.20	4.03	0.6054
2.77	0	-2.67	0	0	0	11.18	4.27	0.6053
2.755	-0.323	-2.576	0.851	-0.977	0.601	12.38	4.683	0.6054

Similarly with the 8 K structure, the V_1 and V_3 are the dominant vectors contributing to the 22 K structure. Only the 4^{th} vector or 6^{th} vector contribute to the peak at ~15 degree, so it's necessary to include either 4^{th} or 6^{th} vector even though V_1+V_3 gives the best agreement. The solution considering V_1, V_3, and V_4 gives comparable agreement factor R_{mag} =12.16 % to the solution considering V_1, V_3 and V_6, R_{mag} =12.20 %. For solution involving the 4^{th} vector, the magnetic moment oscillates between ~1 μ_B to ~5 μ_B. The propagation vector is refined to be $\boldsymbol{k}$=(0, δ,0), δ=0.60543.

$(Mo_{2/3}Er_{1/3})_2AlC$

The NPD pattern of $(Mo_{2/3}Er_{1/3})_2AlC$ at 1.5 K showed additional magnetic reflections emerge compared to the room temperature and 22K patterns. The angular position of these magnetic reflections was obtained by subtracting the 22 K profile from the 1.5 K profile. Attempts to index the magnetic structure using special symmetry points revealed that the reflection at Q ~ 0.37 $Å^{-1}$ can be indexed using the $\mathbf{k_1}$ = (1/2, 0, 1/2) propagation vector, however, a successful indexing of the remaining magnetic reflections using "k-search" turned out to be unsuccessful. This is due to the low resolution of the E6 instrument and the low symmetry of the i-MAX unit cell, which resulted in the overlap of many magnetic reflections. Therefore, a systematic Brillouin zone scan combined with a simulated annealing magnetic refinement was performed as implemented in the SARAh package. For each tested propagation vector the magnetic structure was refined using Monte Carlo optimization with 100 steps per each vector. The refinement parameters were the magnitude and directions of the four Er atoms not related by translational symmetry within the 8f Wyckoff site. The automated scan yielded the $\mathbf{k_2}$ = (0, 0.68, 0) propagation vector as a possible indexing of the magnetic unit cell. Using $\mathbf{k_1}$ and $\mathbf{k_2}$ as starting points, the irreducible representations of the little group were calculated using the BasIreps package. The results for $\mathbf{k_2}$ are the same as with the Tb case. After trying the possible representations, we find that Γ_2 is the correct representation. Refinement of the coefficients of the basis vectors $V_1,\ldots,V_6$ shows that V_4 and V_6 are the dominant vectors. Refining both V_1 and V_3 in addition to the two dominant vectors results in a slightly better agreement. The full results of the refinement are summarized in Table V. The best fit results in a maximal magnetic moment of 5.6(2) μ_B/Er. The value of the propagation vector $\mathbf{k_2}$ = (0, δ, 0) was also refined, resulting in with δ=0.675(1) (Table V). It is worth mentioning that the magnetic scattering of Er_2O_3 (~2 wt.%) was considered.

Table V. Refinement results for different magnetic configurations considered.

V1	V2	V3	V4	V5	V6	R-mag (%)	M (μB)	$\boldsymbol{k}$=(0,δ,0)
0	0	0	2.9920	0	5.3357	11.5	5.4723	0.67622
1.7121	0	0	2.9339	0	5.1005	10.5	6.0418	0.67449
0	0.0063	0	3.0070	0	5.3484	11.4	5.4878	0.67592
0	0	1.4503	2.9017	0	5.0939	10.4	5.4106	0.67384
0.4988	**0**	**1.5223**	**2.9028**	**0**	**5.0938**	**10.3**	**5.6006**	**0.67385**
0	0	0	2.9920	1.4557	5.3513	11.2	5.6754	0.67593

Symmetry analysis of $\mathbf{k_1}$ = (1/2, 0, 1/2) yields two irreducible representations Δ_1 and Δ_2 (Table VI). The 4 Er atoms in the 8f site, that are not related by the base translation C, split into two orbits. For each orbit the decomposition of the magnetic group is $\Delta_m = 3\Delta_1 \oplus 3\Delta_2$. Similarly to the case of $\mathbf{k_2}$, we combine the two orbits in a symmetric and antisymmetric way, leading to a magnetic representation of $\Delta_m = 6\Delta_1 \oplus 6\Delta_2$. Each representation has 6 basis vectors labeled by $W_1,\ldots,W_6$.

Table VI. The irreducible representations of the little group G_k, **k** = (1/2, 0, 1/2).

Irreps	{1}	$\{m_y\|00p\}$
Δ_1	1	-i
Δ_2	1	i

The magnetic configurations that correspond to each basis vector are given in Table VII. Here the relevant Er atoms are chosen to remain inside the basic unit cell, and therefore use unconventional symmetry operators.

Table VII. The magnetic configurations corresponding to each basis vector of Δ_1 and Δ_2.

Irrep.	Basis vector	Er1 (x,y,z)	Er8 (x-1/2,-y+1/2,z+1/2)	Er2 (-x+1,y,-z+1/2)	Er3 (-x+1,-y+1,-z+1)
Δ_1	W_1	[100]	[100]	[100]	[-i00]
	W_2	[010]	[0-10]	[010]	[0i0]
	W_3	[001]	[001]	[001]	[00-i]
	W_4	[100]	[100]	[-100]	[i00]
	W_5	[010]	[0-10]	[0-10]	[0-i0]
	W_6	[001]	[001]	[00-1]	[00i]
Δ_2	W_1	[100]	[-100]	[100]	[i00]
	W_2	[010]	[010]	[010]	[0-i0]
	W_3	[001]	[00-1]	[001]	[00i]
	W_4	[100]	[-100]	[-100]	[-i00]
	W_5	[010]	[010]	[0-10]	[0i0]
	W_6	[001]	[00-1]	[00-1]	[00-i]

A trial and error search has been performed on all basis vectors. Two possible solutions, which agree with the observed data, were found. These are W_5 of representation Δ_1 and W_6 of representation Δ_2. The results of these two configurations are given in Table VIII. The best fit configuration gives a magnetic moment of 0.80(3) μ_B/Er atom.

Table VIII: The refinement results for the possible magnetic configurations of the k_2 propagation vector.

Configuration	M (μ_B)	R-mag (%)
Δ_1, W_5	0.796	11.5
Δ_2, W_6	**0.9889**	**11.2**

Section S7. Structural parameters from NPD

Table S3. Structural refinement from NPD. The global residuals for the refinement of RE=Tb, Rp = 9.60%, Rwp = 14.4%, Re = 1.21%, and χ^2 = 141. For RE=Er, Rp = 1.87%, Rwp = 2.47%, Re = 0.66%, and χ^2 = 13.8.

$(Mo_{2/3}Tb_{1/3})_2AlC$ @100 K	Bragg R = 21.6	RF = 22.3		
C 2/c	*a* = 9.52821 (44)	*b* = 5.51591 (22)	*c* = 14.04858 (86)	β = 103.57702 (282)
	Wyckoff	x	y	z
Mo	8f	0.27038(209)	0.44714(354)	0.07563(116)
Mo	8f	0.60505(212)	0.39864(324)	0.08213(107))
Tb	8f	0.95567(172)	0.41863(328)	0.11074(100)
Al	8f	0.75950(323)	0.15239(624)	0.24360(183)
Al	4e	0	0.92257(924)	0.25
C	8f	0.42383(213)	0.26362(356)	-0.00809(122)
C	4d	0.25	0.25	0.5

$(Mo_{2/3}Er_{1/3})_2AlC$ @320 K	Bragg R = 21.6	RF = 22.3		
C 2/c	*a* = 9.37679 (64)	*b* = 5.45083 (29)	*c* = 13.88838 (125)	β = 103.49207 (612)
	Wyckoff	x	y	z
Mo	8f	0.27287(177)	0.43060(354)	0.08314(72)
Mo	8f	0.61766(169)	0.41526(358)	0.08109(66)
Er	8f	0.95352(148)	0.42417(347)	0.11260(62)
Al	8f	0.74449(297)	0.15634(533)	0.24482(177)
Al	4e	0	0.91914(773)	0.25
C	8f	0.42158(153)	0.23696(292)	-0.01378(69)
C	4d	0.25	0.25	0.5

Reference

1. Palacios, E.; Bartolomé, J.; Luis, F.; Sonntag, R., Nuclear polarization of Nd in the pseudocubic perovskite $NdAlO_3$ studied by neutron diffraction below 1 K. *Phys. Rev. B* **2003**, 68 (22), 224425.

2. Cashion, J.; Cooke, A. H.; Hawkes, J.; Leask, M.; Thorp, T.; Wells, M. R., Magnetic Properties of Antiferromagnetic $GdAlO_3$. *J. Appl. Phys.* **1968**, 39 (2), 1360-1361.

3. Kolmakova, N.; Krynetskii, I.; Lukina, M.; Mukhin, A., Crystal Field and Metamagnetic Behavior of Rare‐Earth Orthoaluminates: $DyAlO_3$. *phys. status solidi (b)* **1990**, 159 (2), 845-850.

4. Hammann, J.; Ocio, M., Electronic and nuclear magnetic ordering in $HoAlO_3$. *J. Mag. Mag. Mater.* **1980**, 15, 39-41.

5. Moon, R.; Child, H.; Koehler, W.; Raubenheimer, L., Magnetic Structure of Er_2O_3 and Yb_2O_3. *J. Appl. Phys.* **1967**, 38 (3), 1383-1383.